Int. J. Heat Mass Transfer. Vol. 27, No. 4, pp. 529–539, 1984
Printed in Great Britain

0017–9310/84 $3.00 + 0.00

MASS TRANSFER DUE TO A CONFINED LAMINAR IMPINGING TWO-DIMENSIONAL JET

HIN-SUM LAW and JACOB H. MASLIYAH
Department of Chemical Engineering, University of Alberta,
Edmonton, Alberta T6G 2G6, Canada

(*Received* 10 *December* 1982 *and in revised form* 18 *July* 1983)

Abstract—Local mass transfer due to impingement of a confined laminar two-dimensional air jet on a flat surface has been studied both experimentally and theoretically for a jet Reynolds number up to 400 and for two different jet-to-plate spacings. The experimental study was carried out via double exposure and real-time holography and the theoretical study was made via the numerical solution of the transport equations. It was found that the span-wise variation of the local Sherwood number exhibits a local minimum and maximum.

NOMENCLATURE

A calibration constant [kg m^{-2}]
b slot width [m]
c concentration of swelling agent [kmol m^{-3}]
c_1 coefficient in equation (10)
C dimensionless concentration of swelling agent, $(c-c_j)/(c_s-c_j)$
d nozzle diameter [m]
D diffusion coefficient [m s^{-2}]
Gz Graetz number, $(Re_{Dh}\ Sc)/(x/2h)$
h jet-to-plate spacing [m]
k local mass transfer coefficient defined in equation (4) [m s^{-1}]
k' local mass transfer coefficient defined in equation (32) [m s^{-1}]
L dimensionless jet-to-plate spacing, h/b
Mw molecular weight of swelling agent [kg kmol^{-1}]
n fringe order
n_p refractive index of glass prism
n_s refractive index of swollen polymer coating
N mass flux [kg m^{-2} s^{-1}]
p partial vapor pressure of swelling agent [kPa]
P total pressure [kPa]
Pr Prandtl number
P° vapor pressure of swelling agent [kPa]
r radial distance measured from the jet center [m]
r' displacement or recession of polymer coating [m]
Re_b Reynolds number for two-dimensional jet, $\bar{v}_j b/\nu$
Re_d Reynolds number for axisymmetric jet, $\bar{v}_j d/\nu$
Re_{Dh} Reynolds number for parallel-plates channel, $2h\bar{u}_o/\nu$
Sc Schmidt number, ν/D
Sh_b Sherwood number, kb/D
Sh_d Sherwood number, kd/D
Sh'_{Dh} Sherwood number, $2hk'/D$
Sh_b° stagnation point Sherwood number
T duration of mass transfer experiment [s]
u streamwise velocity in x-direction [m s^{-1}]
$\bar{u}_o$ mean velocity in x-direction in outflow region [m s^{-1}]
U dimensionless streamwise velocity in x-direction, $u/\bar{v}_j$
UDS upstream differencing scheme
UWDS upstream-weighted differencing scheme
v axial velocity in y-direction [m s^{-1}]
$\bar{v}_j$ mean velocity of jet at nozzle exit [m s^{-1}]
V dimensionless axial velocity in y-direction, $v/\bar{v}_j$
x streamwise distance measured from the jet center [m]
X dimensionless streamwise coordinate, x/b
y axial distance measured from the jet nozzle exit [m]
Y dimensionless axial coordinate, y/b.

Greek symbols

β_1 incident angle of light path travelling from glass prism to polymer coating
β_2 refractive angle of light path travelling from glass prism to polymer coating
λ wavelength of light [m]
μ viscosity of air [kg m^{-1} s^{-1}]
ν kinematic viscosity of air [m^2 s^{-1}]
ρ_s density of swollen polymer coating [kg m^{-3}]
$\bar{\rho}$ molar density of gas mixture [kmol m^{-3}]
ψ stream function [m^2 s^{-1}]
Ψ dimensionless stream function, $\psi/(b\bar{v}_j)$
ω vorticity [s^{-1}]
Ω dimensionless vorticity, $\omega(b/\bar{v}_j)$.

Subscripts

b slot width as characteristic length
B bulk flow
d nozzle diameter as characteristic length

Dh	hydraulic diameter of parallel-plates channel
j	at jet nozzle exit
o	in outflow region
s	at coating surface or impingement plate.

INTRODUCTION

JET IMPINGEMENT flows are frequently used for their excellent heat and mass transfer characteristics, where localized and controlled surface transfer is desirable. The drying of textiles, veneer, paper or film material, the annealing of metal or plastic sheets, the tempering of glass, and the cooling of gas turbine blades or miniature electronic components are some of its more important practical applications. Most studies of impinging jets have been mainly concerned with turbulent jets due to their industrial application. Laminar impinging jets are less commonly used. However, they can be encountered in practice especially when the jet-to-plate spacing is small and a very high stagnation pressure is not desirable.

Heat and mass transfer characteristics of impinging axisymmetric jets (issuing from circular tubes) have been studied rather extensively. The theoretical and experimental findings are well correlated. However, heat and mass transfer characteristics of impinging two-dimensional (2-D) jets (issuing from parallel plates) have received lesser attention. Only few investigators have studied theoretically or experimentally the heat and mass transfer due to a laminar impinging 2-D jet [1–6]. Of these studies, only the numerical study by van Heiningen *et al.* [5] considered the effect of the presence of a confinement plate.

The objective of this work is to study both experimentally and numerically the mass transfer characteristics of a confined laminar jet impinging on a flat plate.

EXPERIMENTAL PROCEDURE

The suitability of the swollen polymer method coupled with a laser holography interferometric technique for local mass transfer measurements has been demonstrated by previous investigators [7–11]. Details of this technique have already been given by Macleod and Todd [7] and Masliyah and Nguyen [10] and will not be repeated here.

The arrangement of the experimental setup of this study is shown in Fig. 1. A concrete table 2.74 × 1.37 × 0.13 m was used as the work surface for the experimental setup. The positions of the optical components and the polymer coating, shown in Fig. 1, were determined according to the Holo-Diagram technique [12]. By using the right-angle glass prism as the base for the impingement surface, it allowed the entire optical setup to be located behind the mass transferring surface. Such an arrangement is suitable not only for double exposure holographic interferometry but also for real-time holographic interferometry.

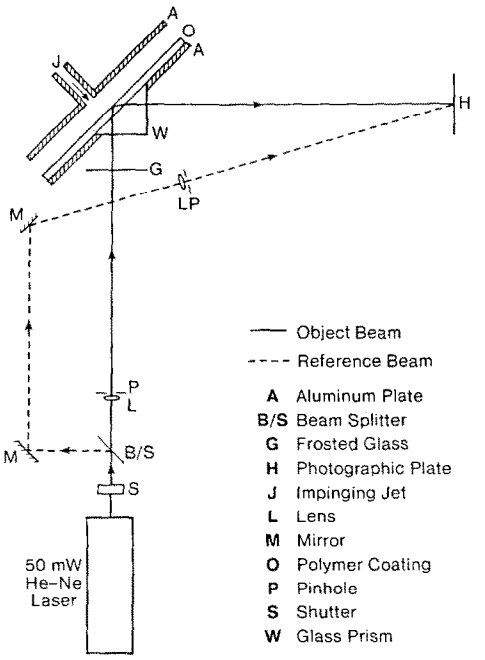

FIG. 1. Arrangement of the experimental setup.

The hypotenuse surface of a right-angle prism (0.089 × 0.125 m) was fitted into a window cutting of an aluminum plate (0.625 × 0.149 × 0.012 m). The glass surface of the prism together with the aluminum plate formed a smooth surface which was then coated with a thin layer of silicone rubber to become the mass transferring surface or the impingement plate. The confinement plate was an aluminum plate (0.625 × 0.149 × 0.012 m) to which the jet tube was attached. The jet tube was 0.4 × 0.132 × 0.0015 m and its length of 0.4 m was long enough to provide a fully developed profile at the nozzle exit for the highest Reynolds number used in this study.

Two sets of spacers were used to fit between the impingement and the confinement plates so as to permit two jet-to-plate spacings and to form a rectangular channel to which the jet flow would be confined.

Normally, holographic interferometry is made using a double exposure. Details of this method has been given by Kapur and Macleod [8, 9] and Masliyah and Nguyen [6, 10, 11]. The so-called 'frozen fringe pattern' formed by the reconstruction of a double exposed hologram, indicates contours of equal surface recession or equal mass transfer. From the geometry of the optical setup, it is possible to evaluate the coating shrinkage between two consecutive fringes [8, 10]. Figure 2 shows the paths of a light ray before and after a mass transfer experiment for a given change of coating thickness, r'. The change in the light path length between a–a and b–b is the same as that between c–c and d–d, and is given by

$$2r'(n_s - n_p \sin \beta_1 \sin \beta_2)/\cos \beta_2, \qquad (1)$$

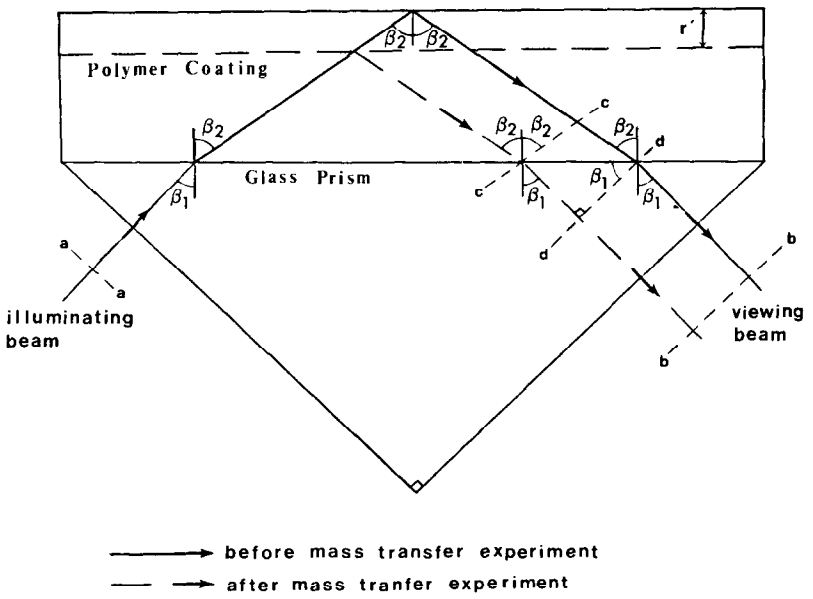

FIG. 2. Light path length before and after mass transfer.

where n_s and n_p are the refractive index of the swollen polymer and the glass prism, respectively ($n_s = 1.428$ and $n_p = 1.50$). The angle β_1 as shown in Fig. 2 is equal to 45°. The angle $\beta_2 = \sin^{-1}(n_p \sin \beta_1/n_s)$ is calculated as 47°58′. As the appearance of a fringe is due to a change of light path length of $n\lambda/2$, then the change of coating thickness r' for the nth fringe is given by

$$r' = n\lambda \cos \beta_2/4(n_s - n_p \sin \beta_1 \sin \beta_2). \quad (2)$$

Hence, by knowing the wavelength of the light, λ and by determining the fringe order, n, the absolute magnitude of the polymer coating shrinkage at a given point can be evaluated.

Some basic methods for determining local fringe order such as zero fringe identification were mentioned by Masliyah and Nguyen [10]. Due to the presence of local extrema in Sherwood number, a more complicated 'frozen fringe pattern' is to be expected. In such a case, in order to determine the local fringe order, the methods used by Masliyah and Nguyen are no longer applicable and therefore real-time holographic interferometry is used. Detail of the real-time holographic interferometric technique has been given by Law [13]. In this technique, the order of any particular fringe at any given time can be easily determined by counting the fringes at a given location as they appear in real time. In order to determine the fringe order of the 'frozen fringe pattern', a duplicate experimental run is made using real-time holography.

The mass transfer experiments were conducted with the coating surface subjected to the air jet for a period of T, ranging from 120 to 480 s. The range of Reynolds number was 100–400 with the slot width, b, taken as the characteristic length. The jet-to-plate spacings were $2b$ and $4b$. The Schmidt number of the ethylsalicylate–air system is 2.74 at 21°C. The results of the various mass transfer experiments are presented in terms of local Sherwood number, defined by

$$Sh_b = kb/D, \quad (3)$$

where k is defined by

$$N = k(p_s - p_i)\bar{\rho} Mw/P. \quad (4)$$

Here N is the mass flux, $\bar{\rho}$ is the molar density of the gas mixture, Mw is molecular weight of the swelling agent, P is the total pressure and p_s and p_j are the partial vapor pressures of the swelling agent at the coating surface and at the jet nozzle exit, respectively. Since $p_j = 0$ for an air jet and $p_s = P°$, for a 'constant rate period' [7], equation (4) becomes

$$N = kP°\bar{\rho} Mw/P. \quad (5)$$

The mass flux, N, can also be given as [7]

$$N = r'\rho_s/T, \quad (6)$$

where r' is the change of coating thickness given by equation (2), ρ_s is the density of the swollen polymer and T is the duration of the mass transfer experiment. Substituting equation (2) into equation (6), one obtains

$$N = A(n/T), \quad (7)$$

where

$$A = \lambda\rho_s \cos \beta_2/4(n_s - n_p \sin \beta_1 \sin \beta_2), \quad (8)$$

and is a constant for a given mass-transferring system and optical setup. Constant A is also referred to as the calibration constant of the experimental setup. Combining equations (3), (5) and (7), one obtains

$$Sh_b = (AP/\bar{\rho}P°Mw)(n/T)(b/D). \quad (9)$$

Therefore, it is necessary to know the physical properties, the local fringe order and the duration of the mass transfer experiment in order to evaluate the local Sherwood number. From equation (8), the calibration constant A becomes 1.67×10^{-4} kg m^{-2}.

An alternative way to obtain the calibration constant A was suggested by Masliyah and Nguyen [10] by studying the mass transfer due to an unconfined laminar impinging axisymmetric air jet with an initial parabolic velocity profile using the same optical setup of Fig. 1. This calibration is made using the theoretical expression derived from the exact solution of Scholtz and Trass [14] for an unconfined laminar impinging axisymmetric jet in the wall jet region

$$k = c_1\, Re_d^{0.75}(r/d)^{-1.25}, \tag{10}$$

where

$$c_1 = 0.458(D/d)\Gamma(Sc+1/3)/(\Gamma(Sc)\Gamma(1/3)), \tag{11}$$

for the initial parabolic velocity profile. It is noted that in equation (11), the Schmidt number is explicitly included in terms of the gamma functions as suggested by other investigators who studied wall jets [1, 14]. From equations (3), (9) and (10), and interchanging the slot width, b, with the nozzle diameter, d, one obtains

$$n = (c_1\bar{\rho}P^{\circ}Mw/AP)(T\, Re_d^{0.75}(r/d)^{-1.25}). \tag{12}$$

If a mass transfer experiment is performed using an unconfined impinging axisymmetric air jet with an initial parabolic velocity profile, then a plot of n vs $(T\, Re_d^{0.75}(r/d)^{-1.25})$ in the wall jet region gives as its slope $(c_1\bar{\rho}P^{\circ}Mw/AP)$. The constant A can then be evaluated from the knowledge of the physical properties of the system.

The experimental setup for an unconfined axisymmetric jet is similar to that for a confined 2-D jet mentioned above. The confinement plate and the slot tube was replaced by a circular tube with a diameter equal to 0.003 m. The jet-to-plate spacing was $1.5d$. Double exposure holographic interferometry was used throughout this calibration. Experimental runs with $T = 90$, 180 and 360 s and for $Re_d = 1210$ and 1470 were made.

From the results of this calibration, the slope of the least squares linear regression of n vs $(T\, Re_d^{0.75}(r/d)^{-1.25})$ is 634.08 s^{-1} which gives A as 1.614 $\times 10^{-4}$ kg m^{-2} using the physical properties given in the Appendix. The agreement between the two methods for evaluating the constant A is within 3.3%. The value of A obtained from an unconfined axisymmetric air jet is used for the evaluation of local Sherwood number throughout the experimental study of this work.

It is appropriate to mention that the major shortcoming of this technique is that it is not suitable for determining local mass transfer in a region where rapid change in mass transfer occurs (e.g. stagnation flow region). This is mainly due to the difficulty in identifying the very fine fringes in this region.

NUMERICAL SIMULATION

A 2-D numerical model is used to simulate the experimental setup. The impinging jet system considered in this work is shown in Fig. 3. The air jet issues from a slot tube of width b with an average velocity of $\bar{v}_j$. The confinement plate is located parallel to and at a distance h from the impingement plate. The origin of the 2-D coordinate system is located at the center of the jet nozzle exit. The x-coordinate is parallel to the impingement plate and the y-coordinate is normal to it. The outflow region is chosen at a location sufficiently far away from the stagnation flow region that the developing velocity and concentration profiles are as for a parallel-plates channel.

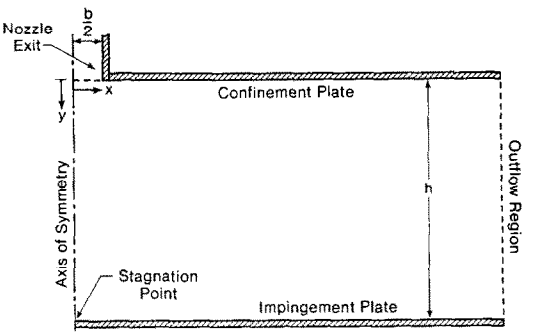

FIG. 3. Coordinate system and boundaries of the jet system.

The 2-D momentum and transport equations can be reduced to the corresponding vorticity–stream function form with the assumptions of steady-state, incompressible viscous Newtonian fluid flow with constant physical properties. The pertinent equations are

$$\frac{\partial(U\Omega)}{\partial X} + \frac{\partial(V\Omega)}{\partial Y} = \frac{1}{Re_b}\left(\frac{\partial^2\Omega}{\partial X^2} + \frac{\partial^2\Omega}{\partial Y^2}\right), \tag{13}$$

$$\frac{\partial^2\Psi}{\partial X^2} + \frac{\partial^2\Psi}{\partial Y^2} = \Omega, \tag{14}$$

$$\frac{\partial(UC)}{\partial X} + \frac{\partial(VC)}{\partial Y} = \frac{1}{Re_b\, Sc}\left(\frac{\partial^2 C}{\partial X^2} + \frac{\partial^2 C}{\partial Y^2}\right). \tag{15}$$

All the variables in equations (13)–(15) are dimensionless and are defined as

$$\begin{aligned} &L = h/b, \\ &U = u/\bar{v}_j, \qquad V = v/\bar{v}_j, \\ &X = x/b, \qquad Y = y/b, \\ &C = (c-c_j)/(c_s-c_j), \\ &\Omega = \omega(b/\bar{v}_j), \qquad \Psi = \psi/(b\bar{v}_j), \\ &Re_b = b\bar{v}_j/\nu, \qquad Sc = \nu/D. \end{aligned} \tag{16}$$

The stream function is defined by

$$\frac{\partial\Psi}{\partial Y} = U, \qquad \frac{\partial\Psi}{\partial X} = -V. \tag{17}$$

The objective of the numerical study is to solve equations (13)–(15) for Ω, Ψ and C. Because the equations are elliptic in nature, boundary conditions must be specified at all the boundaries. The boundaries are specified for five regions.

Nozzle exit

From the fully developed velocity profile between two parallel plates one can derive

$$\Psi = -1.5X + 2X^3, \tag{18}$$

$$\Omega = 12X, \tag{19}$$

and

$$C = 0 \text{ (zero swelling agent concentration).} \tag{20}$$

Confinement plate

Because the confinement plate is impermeable, the value of the stream function does not change along the plate. This value can be determined by substituting $X = 0.5$ in equation (18) to give

$$\Psi = -0.5. \tag{21}$$

The boundary condition for the vorticity at the confinement plate is approximated by a finite-difference expression which embodies the no-slip conditions: $\partial\Psi/\partial Y = U = 0$ and $\partial^2\Psi/\partial^2 Y = \partial U/\partial Y = \Omega$ at the boundary. The boundary condition for the concentration is

$$\frac{\partial C}{\partial Y} = 0 \quad \text{(zero mass flux).} \tag{22}$$

Impingement plate

Again, because the impingement plate is impermeable, the value of the stream function does not change along the plate, and its value is given by

$$\Psi = 0. \tag{23}$$

The boundary condition of the vorticity at the impingement plate is the same as that of the confinement plate. The boundary condition for the concentration is

$$C = 1. \tag{24}$$

Axis of symmetry

Along the axis of symmetry the boundary conditions are

$$\Psi = 0, \tag{25}$$

$$\Omega = 0, \tag{26}$$

and

$$\frac{\partial C}{\partial X} = 0. \tag{27}$$

Outflow region

Developing flow and concentration profiles as for a parallel-plates channel are assumed for this boundary. The developing stream function and vorticity profiles are derived from the developing velocity profile given by Sparrow *et al.* [15]. The developing concentration profile is analogous to the developing temperature profile for parallel plates given by McCuen [16]. The location of this boundary was chosen at $X_{max} = 74$.

The local mass transfer flux is given by

$$N = k(c_s - c_j)Mw \tag{28}$$

$$= DMw\left(\frac{\partial c}{\partial y}\right)\Big|_{y=h}, \tag{29}$$

which leads to

$$Sh_b = \frac{\partial C}{\partial Y}\Big|_{Y=L}. \tag{30}$$

An alternative definition for the Sherwood number can be given as

$$Sh'_{Dh} = \frac{2hk'}{D}, \tag{31}$$

where

$$N = k'(c_s - c_B)Mw. \tag{32}$$

Here c_B is the bulk flow concentration defined as

$$c_B = \left(\int_0^h uc\,dy\right)\Big/(\bar{u}_o h), \tag{33}$$

where $\bar{u}_o$ is the average velocity in the outflow region and is equal to $\frac{1}{2}\bar{v}_j b/h$. The alternative Sherwood number definition is more suitable in the outflow region of the parallel plates. Introducing the dimensionless variables of equation (16), one obtains

$$Sh'_{Dh} = 2L\left(\frac{\partial C}{\partial Y}\right)\Big|_{Y=L}\Big/(C_s - C_B), \tag{34}$$

where

$$C_B = 2\int_0^L UC\,dY. \tag{35}$$

It should be mentioned here, that Sh'_{Dh} is not evaluated experimentally due to the difficulty in measuring C_B and Sh'_{Dh} is only given using the numerical analysis.

The approximation of a convection–diffusion differential equation by hybrid differencing schemes (upstream-weighted and upstream differencing schemes) used in this study is described in detail by Raithby and Torrance [17] and will not be repeated here. A non-uniform grid is used throughout the numerical computations in this work. Due to the relatively large gradients of velocity and concentration along the impingement plate, the gridlines parallel and adjacent to this plate must be very closely spaced. Also, gridlines parallel and adjacent to the axis of symmetry are closely spaced in order to ensure accurate calculation of the variables within the stagnation flow region.

A grid network of 55×25 was used. The number of gridlines in the x-direction was 55 with 9 gridlines covering the distance between $X = 0$ and 0.5. The number of gridlines in the y-direction was 25.

The Gauss–Seidal iteration method coupled with the conventional successive over relaxation (SOR) method was used to solve the finite-difference equations. A modified scheme of the calculation, presented by

Wilkes [18] was used during the iteration procedure. This modified scheme has been observed by Masliyah and Nandakumar [19] to have a stabilizing effect on the convergence characteristics and it is twice as fast as the conventional SOR method. Convergence of the numerical results was assumed when the maximum absolute difference between two consecutive iterations was within 10^{-4} for the vorticity and stream function and 10^{-6} for the concentration.

The suitability of the convergence criteria together with the grid network was confirmed by numerical experimentation.

RESULTS AND DISCUSSION

The main objective of this paper is to study the mass transfer characteristics. However, because of the close inter-relation between mass transfer and the flow field [13], the latter will be considered briefly.

The flow field is studied qualitatively by observing the streamline contours from the numerical solution. The contours of the stream function for $L = 4$ are shown in Fig. 4. The jet nozzle exit is at the upper left hand corner with the main flow travelling from left to right. The upper horizontal streamline represents the confinement plate and the lower horizontal streamline represents the impingement plate. In general, a primary vortex rotating in the counter-clockwise direction is found near the confinement plate with its size increasing with jet Reynolds number. With the exception of the case of low Reynolds numbers for $L = 2$, a second vortex rotating in the clockwise direction is found near the impingement plate. This secondary vortex is much smaller than the first one in size and it is also weaker in terms of rotational intensity. It can be observed in Fig. 4 that the centers of both the primary and the secondary vortices move downstream with an increase in Reynolds number. It is shown later that the presence of local extrema in the Sherwood number are attributed to the flow recirculation in the region between the confinement and the impingement plates.

A typical 'frozen fringe pattern' due to mass transfer from a flat plate under the influence of a confined laminar impinging 2-D jet for $Re_b = 306$ and $L = 2$ is shown in Fig. 5. These fringes are interpreted as contours of equal mass transfer rate. The presence of a local minimum and a local maximum in the mass transfer rate can be observed in the outer region. Local mass transfer rates are measured along the centerline of the impingement plate where the local fringes in this region are nearly parallel to each other.

Typical comparisons between the experimental and the numerical results are shown in Figs. 6 and 7 for $L = 2$ and 4, respectively. Excellent agreement is obtained between the experimental and the numerical results. Furthermore, the numerical results confirm the presence of local extrema in the Sherwood number. The numerical results from the upstream-weighted differencing scheme (UWDS) gave a better prediction

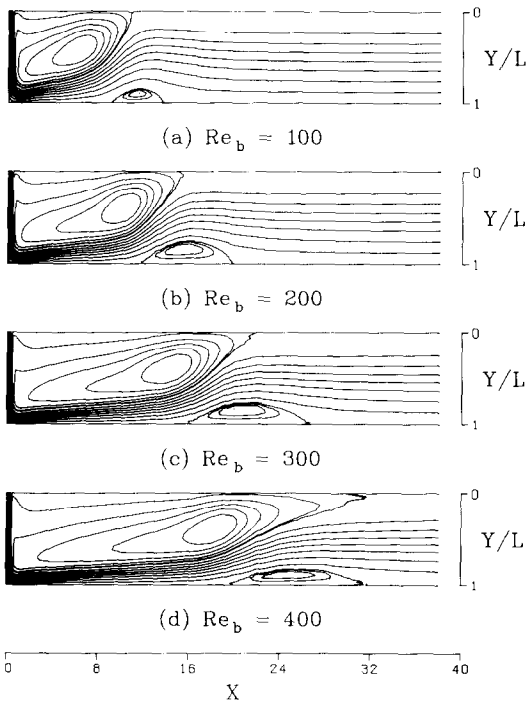

FIG. 4. Contours of stream function ($L = 4$).

than the upstream differencing scheme (UDS) as would be expected [17].

The variations of the local Sherwood number along the impingement plate for different Reynolds numbers are shown in Fig. 8 for $L = 4$ using the numerical results from the UWDS. The maximum Sherwood number is found to occur close to the stagnation point for all cases.

In general, the variation of the local Sherwood number along the impingement plate for a confined 2-D jet can be classified into five regions. The five regions are shown in Fig. 9 for the case of $L = 4$ and $Re_b = 200$. Also shown in Fig. 9 are the contours of the stream function which indicate a close inter-relation between the flow field and the local Sherwood number. The five regions are:

(1) A stagnation flow region, where local Sherwood number remains fairly constant. This region is directly below the jet nozzle exit ($X \leqslant 0.5$).

(2) A transition region, where local Sherwood number decreases gently from its plateau value. A smooth transition of local Sherwood number from the stagnation flow region to the wall jet region is observed.

(3) A wall jet region, where $\log(Sh_b)$ decreases linearly with $\log(X)$. As shown in Fig. 8, the range of this region is a function of the jet Reynolds number, Although not shown in Fig. 8, the range of this region is also a function of the jet-to-plate spacing as well.

(4) A flow separation region, where the local Sherwood number is found to exhibit a local minimum and a local maximum. Contours of the stream function of Fig. 9 indicate that the presence of these extrema is attributed to flow separation along the impingement

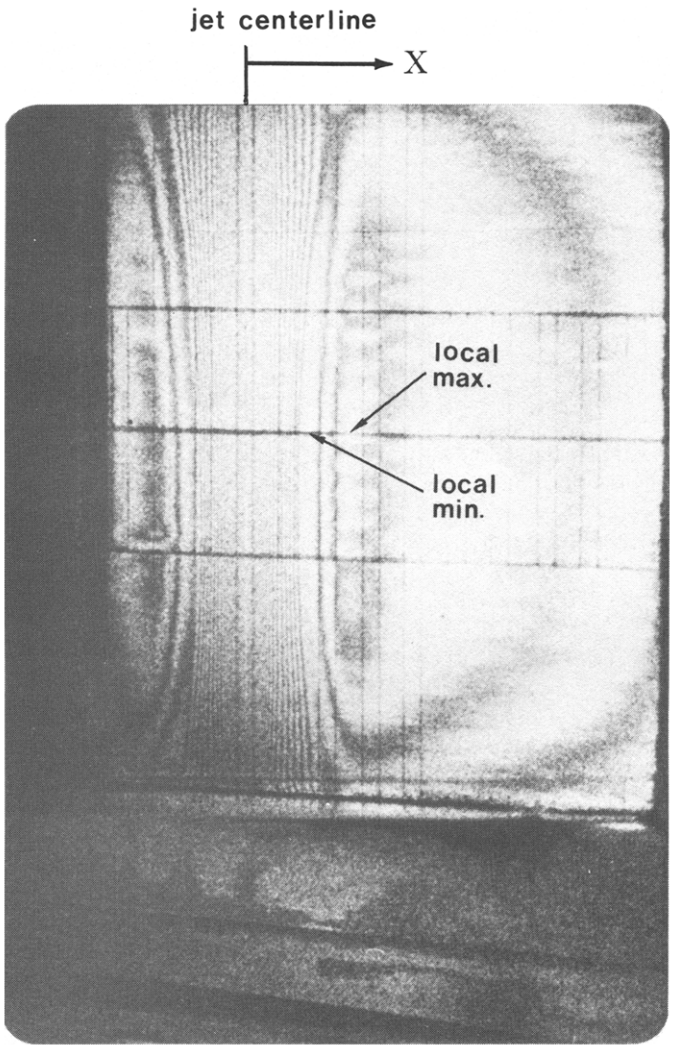

FIG. 5. Contours of equal mass transfer rate for $L = 2$ and $Re_b = 306$.

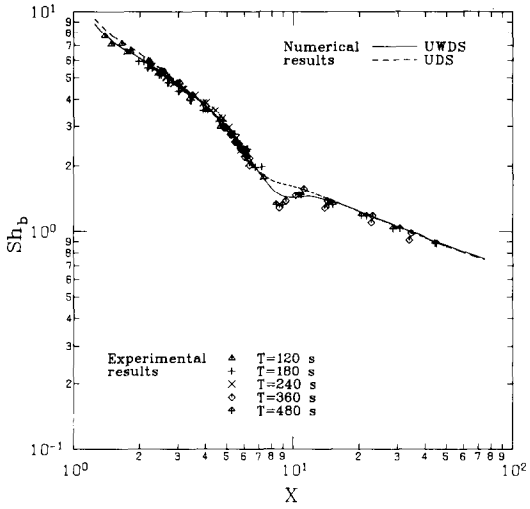

FIG. 6. Comparison of experimental and numerical results for $L = 2$ and $Re_b = 200$.

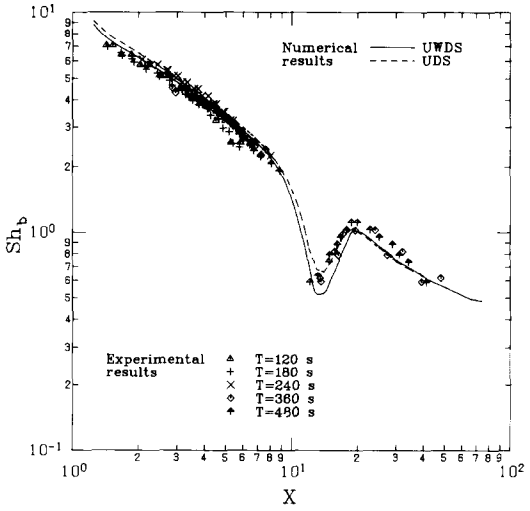

FIG. 7. Comparison of experimental and numerical results for $L = 4$ and $Re_b = 200$.

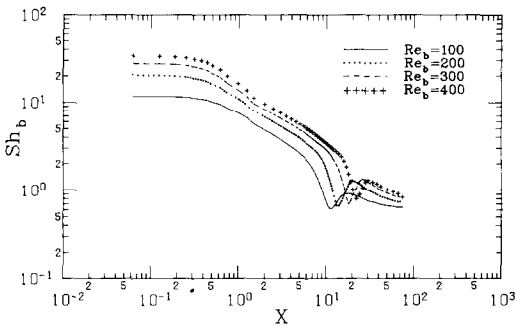

FIG. 8. Variation of local Sherwood number ($L = 4$).

plate. The streamwise location of the secondary vortex center and the streamwise location of the local minimum of the Sherwood number are found to be nearly the same. This indicates that there is a strong correlation between the streamwise location of the secondary vortex and the local minimum in the Sherwood number.

(5) A developing channel flow region, where local Sherwood number develops in the same manner as that for parallel-plates channel flow. The local Sherwood number approaches a constant value as the flow becomes fully developed.

The first three regions for a confined 2-D jet are quite similar to those for an unconfined jet. But the flow separation and the developing channel flow regions are unique for a confined jet since for an unconfined jet, the local Sherwood number eventually approaches zero in the wall jet region.

Comparison of stagnation point Sherwood number evaluated numerically from UWDS with those in the literature is shown in Fig. 10. The heat transfer results of van Heiningen *et al.* [5] were converted to the corresponding mass transfer values by employing a heat–mass transfer analogy as $Sh_b = (Sc/Pr)^{0.4}\, Nu_b$.

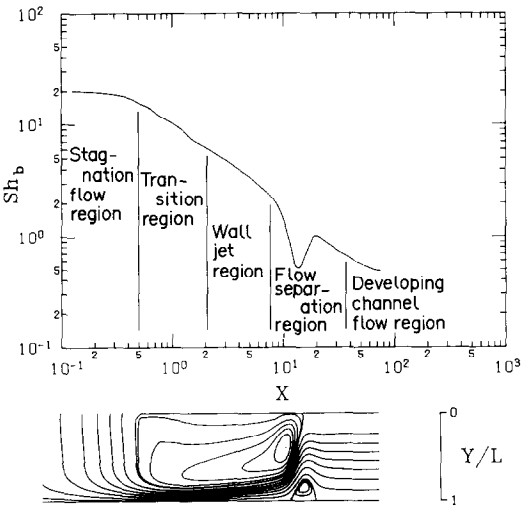

FIG. 9. Classification of mass transfer regions ($L = 4$, $Re_b = 200$).

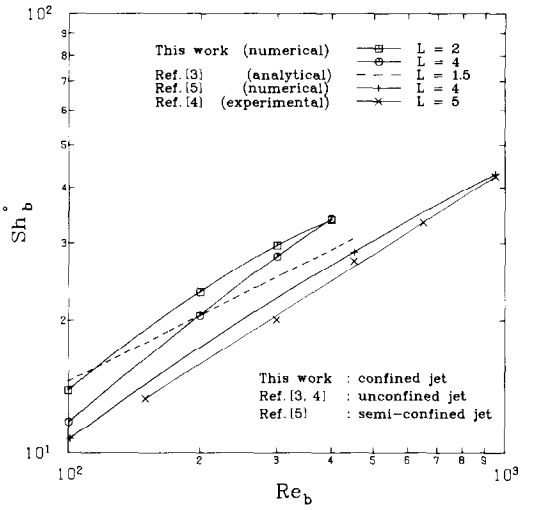

FIG. 10. Comparison of stagnation point Sherwood number with literature ($Sc = 2.74$).

The mass transfer results of Sparrow and Lee [3] and Sparrow and Wong [4] were also converted to the corresponding values for $Sc = 2.74$ by employing a dependency of mass transfer of $Sc^{0.4}$. Little effect of the presence of a confinement plate on the stagnation point heat transfer was claimed by van Heiningen *et al.* [5] due to the good agreement between their results and those of Sparrow and Wong [4] who studied an unconfined jet. But the effect of the confinement plate may be quite significant due to the disagreements between the results for $L = 4$ of this work and those of the two studies mentioned above. It was observed that a confined submerged jet with an initial parabolic profile contracts slightly below the nozzle exit [5, 13]. The result is that the centerline axial velocity decays much slower compared with an unconfined jet. Consequently, the higher centerline axial velocity near the stagnation point results in a higher mass transfer rate. Unfortunately, the stagnation point Sherwood number computed in this work cannot be verified experimentally due to the difficulty in measuring the mass transfer rate at the stagnation point. Therefore, a further study in the stagnation flow region for a confined 2-D jet is recommended.

A regression equation is developed from the experimental data for both $L = 2$ and 4 in the wall jet region. The range of data points used is within the region where $\log(Sh_b)$ vs $\log(X)$ is linear. In this wall jet region, little effect of jet-to-plate spacing on the local Sherwood number is observed. The regression analysis is made in such a way that each data point has approximately the same weighting.

The regression equation for $L = 2$ and 4 is given by

$$Sh_b = 0.34 Re_b^{0.66} X^{-0.78}, \tag{36}$$

for $100 \leqslant Re_b \leqslant 400$ with an average error of 6.8%. The experimental error is associated with the uncertainty of the precise location of the fringes during the analysis of the coarse part of the 'frozen fringe pattern' and also

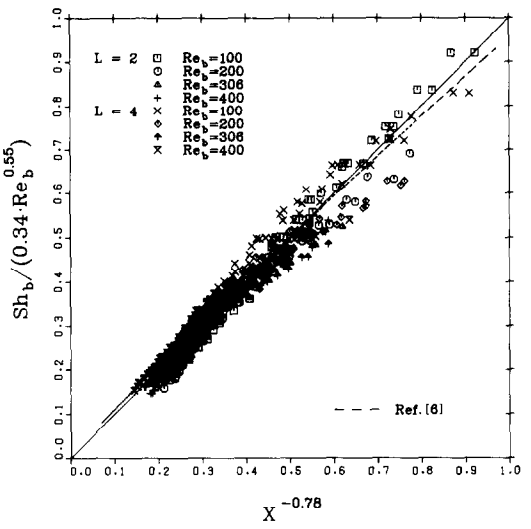

FIG. 11. Test of goodness of fit for equation (36).

with the assumption of a 'constant rate period' in using the swollen polymer method [7]. A total of 685 data points are used. A plot to test the applicability of equation (36) is shown in Fig. 11. For a perfect fit with zero experimental error, all data points should lie on a straight line having a slope of unity. In addition, the results obtained by Masliyah and Nguyen [6] for unconfined 2-D jets with $L = 4$ and 8 are also plotted in Fig. 11 as a dashed line. Their data are well within the range of the experimental error of this work. This indicates that there is little effect of the confinement plate in the wall jet region. However, the effect of a confinement plate is obvious in the fourth region where the extrema of local Sherwood number occur.

The exponent of X', -0.78, in equation (36) is in fair agreement with the experimental findings by Masliyah and Nguyen [6] of -0.73 for an unconfined 2-D jet, and the analytical solutions by Schwarz and Caswell [1] of -0.75 for a 2-D wall jet. Although the exponent of Re_b, 0.66, in equation (36) does not agree with either study, it is within the range of their values of 0.55 and 0.75.

Comparison of local Sherwood number evaluated numerically using UWDS with those for parallel-plates channel flow [16] is shown in Fig. 12 for $L = 4$. A plot of Sh'_{Dh} vs the reciprocal of the Graetz number leads to the collapse of the curves for different Reynolds numbers to a general curve in the outflow region. The Graetz number, Gz, is defined as

$$Gz = \frac{Re_{Dh}\, Sc}{(x/2h)}, \tag{37}$$

where

$$Re_{Dh} = \frac{2hu_o}{\nu} = Re_b. \tag{38}$$

A similar observation is also made for $L = 2$. The general curve approaches the fully developed value of $Sh'_{Dh} = 4.861$ in a manner similar to that for parallel-plate channel flow [16].

CONCLUDING REMARKS

Local Sherwood number along the impingement plate for a confined 2-D jet is found to behave quite differently to that for an unconfined jet in the region far away from the stagnation point. In this region, local Sherwood number is found to exhibit a local minimum and a local maximum. The location of these extrema is a function of jet Reynolds number and jet-to-plate spacing. A 2-D numerical model with the upstream-weighted differencing scheme is found to be very successful in predicting the mass transfer due to a confined 2-D laminar impinging jet.

Acknowledgements—The authors are indebted to the National Science and Energy Research Council of Canada for financial support.

REFERENCES

1. W. H. Schwarz and B. Caswell, Some heat transfer characteristics of the two-dimensional laminar incompressible wall jet, *Chem. Engng Sci.* **16**, 338–351 (1961).

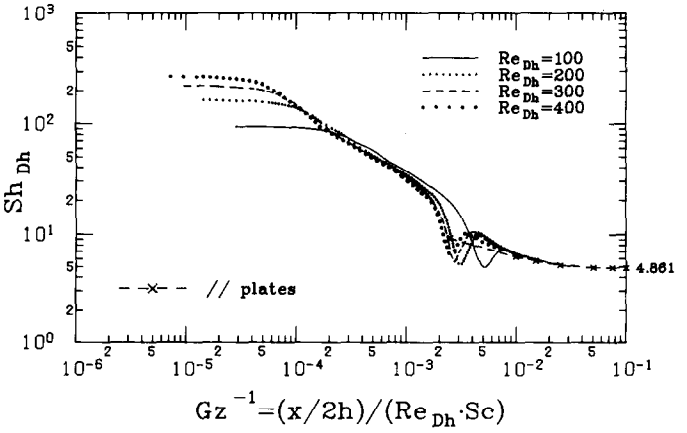

FIG. 12. Variation of Sherwood number with the reciprocal of the Graetz number ($L = 4$).

2. H. Miyazaki and E. Silberman, Flow and heat transfer on a flat plate normal to a two-dimensional laminar jet issuing from a nozzle of finite height, *Int. J. Heat Mass Transfer* **15**, 2097–2107 (1972).
3. E. M. Sparrow and L. Lee, Analysis of flow field and impingement heat/mass transfer due to a nonuniform slot jet, *J. Heat Transfer* **97**, 191–197 (1975).
4. E. M. Sparrow and T. C. Wong, Impingement transfer coefficients due to initially laminar slot jets, *Int. J. Heat Mass Transfer* **18**, 597–605 (1975).
5. A. R. P. van Heiningen, A. S. Mujumdar and W. J. M. Douglas, Numerical prediction of the flow field and impingement heat transfer due to a laminar slot jet, *J. Heat Transfer* **98**, 654–658 (1976).
6. J. H. Masliyah and T. T. Nguyen, Mass transfer due to an impinging slot jet, *Int. J. Heat Mass Transfer* **22**, 237–244 (1979).
7. N. Macleod and R. B. Todd, The experimental determination of wall-fluid mass transfer coefficients using plasticized polymer surface coatings, *Int. J. Heat Mass Transfer* **16**, 485–504 (1973).
8. D. N. Kapur and N. Macleod, The determination of local mass transfer coefficients by holographic interferometry—I, *Int. J. Heat Mass Transfer* **17**, 1151–1162 (1974).
9. D. N. Kapur and N. Macleod, Holographic determination of local mass transfer coefficients at a solid–liquid boundary, *A.I.Ch.E. Jl* **21**, 184–187 (1975).
10. J. H. Masliyah and T. T. Nguyen, Holographic determination of mass transfer due to impinging square jet, *Can. J. Chem. Engng* **54**, 299–304 (1976).
11. J. H. Masliyah and T. T. Nguyen, Experimental study of mass transfer due to an impinging rectangular jet, *Can. J. Chem. Engng* **55**, 156–160 (1977).
12. N. Abramson, The Holo-Diagram: a practical device for making and evaluating holograms, *Appl. Optics* **8**, 1235–1240 (1969).
13. H. S. Law, Mass transfer due to a confined laminar impinging two-dimensional jet, Ph.D. thesis, University of Alberta, Edmonton, Alberta (1982).
14. M. T. Scholtz and O. Trass, Mass transfer in the laminar radial wall jet, *A.I.Ch.E. Jl* **9**, 548–554 (1963).
15. E. M. Sparrow, S. H. Lin and T. S. Lundgren, Flow development in the hydrodynamic entrance region of tubes and ducts, *Physics Fluids* **7**, 338–347 (1964).
16. P. A. McCuen, Heat transfer with laminar and turbulent flow between parallel planes with constant and variable wall temperature and heat flux, Ph.D. thesis, Stanford University, Stanford, California (1961).
17. G. D. Raithby and K. E. Torrance, Upstream-weighted differencing schemes and their application to elliptic problem involving fluid flow, *Comput. Fluid* **2**, 191–206 (1974).
18. M. V. Wilkes, *A Short Introduction to Numerical Analysis*, p. 74. Cambridge University Press, Cambridge (1966).
19. J. H. Masliyah and K. Nandakumar, Fluid flow and heat transfer in internally finned helical coils, *Can. J. Chem. Engng* **55**, 27–36 (1977).

APPENDIX

Density of swollen polymer, $\rho_s = 1.01 \times 10^3$ kg m^{-3}
Molecular weight of ethylsalicylate, $Mw = 166.17$ kg kmol^{-1}
Wavelength of laser light, $\lambda = 632.8 \times 10^{-9}$ m
Vapor pressure of ethylsalicylate, P° (at 21°C and 93.9 kPa) = 0.00843 kPa
Molar density of gas mixture, $\bar{\rho}$ (at 21°C and 93.9 kPa) = 0.0385 kmol m^{-3}
Viscosity of air, μ (at 21°C and 93.9 kPa) = 1.817×10^{-5} kg (ms)$^{-1}$
Diffusion coefficient, D (at 21°C and 93.9 kPa) = 5.95×10^{-6} m^2 s^{-1}

TRANSFERT MASSIQUE DU A L'IMPACT D'UN JET BIDIMENSIONNEL LAMINAIRE CONFINE

Résumé—Le transfert massique dû à l'impact d'un jet d'air bidimensionnel, laminaire et confiné, sur une surface plane est étudié à la fois expérimentalement et théoriquement pour un nombre de Reynolds de jet allant jusqu'à 400 et pour deux distances jet-à-plan. L'étude experimentale est conduite par holographie en temps réel et double exposition et l'étude théorique est faite numériquement à partir des équations de transport. On trouve que la variation spatiale du nombre de Sherwood révèle localement un minimum et un maximum.

STOFFÜBERTRAGUNG BEI EINEM BEGRENZTEN LAMINAR AUFTREFFENDEN ZWEIDIMENSIONALEN STRAHL

Zusammenfassung—Es wurde der örtliche Stoffübergang beim Auftreffen eines begrenzten laminaren zweidimensionalen Luftstrahls auf eine ebene Oberfläche sowohl experimentell als auch theoretisch für Strahl–Reynolds-Zahlen bis 400 und für zwei unterschiedliche Abstände vom Strahl zur Platte untersucht. Die experimentellen Untersuchungen wurden mit Hilfe von Doppelbelichtungs- und Echtzeit-Holografie ausgeführt. Die Ergebnisse der theoretischen Berechnungen wurden mit Hilfe numerischer Lösung der Transportgleichungen gefunden. Es stellte sich heraus, daß die abschnittsweise veränderliche örtliche Sherwood-Zahl ein örtliches Minimum und Maximum zeigt.

МАССОПЕРЕНОС, ОБУСЛОВЛЕННЫЙ НАТЕКАНИЕМ НА ПРЕГРАДУ ОГРАНИЧЕННОЙ В СЕЧЕНИИ ЛАМИНАРНОЙ ДВУМЕРНОЙ СТРУИ

Аннотация—Экспериментально и теоретически изучается локальный массоперенос, обусловленный натеканием на плоскую поверхность ограниченной в сечении ламинарной двумерной струи воздуха при значениях числа Рейнольдса для струи до 400 и при двух различных расстояниях между струей и пластиной. Экспериментальное исследование проводилось с помощью голографирования методом двойного экспонирования в реальном масштабе времени, а теоретическое исследование — путем численного решения уравнений переноса. Найдено, что в распределении локального числа Шервуда по размаху струи имеют место локальные минимум и максимум.